Contract No.:

This manuscript has been authored by Battelle Savannah River Alliance (BSRA), LLC under Contract No. 89303321CEM000080 with the U.S. Department of Energy (DOE) Office of Environmental Management (EM).

The Effect of Radiation Damage on the Charge Collection Efficiency of Silicon Avalanche Photodiodes

Robert M. Zedric, *Member, IEEE*, Craig M. Marianno, Sunil S. Chirayath, Yacouba Diawara, Iain Darby, *Member, IEEE*

***Abstract*— Understanding radiation effects on avalanche photodiodes (APDs) is important because they are used in several applications involving harsh radiation environments. APDs are used as photosensors in applications where speed and detection efficiency are critical. Proton irradiation experiments on a commercial off-the-shelf APD demonstrated that the irradiation flux and applied reverse bias have a strong influence on the severity of radiation effects. This is measured using the ion beam induced charge (IBIC) technique in which charge collection efficiency (CCE) describes the signal response from a device. CCE can degrade substantially due to radiation damage, but recent measurements show that certain combinations of irradiation flux and reverse bias can lead to increases in CCE up to 186 ± 24% for irradiations with 2 MeV protons at a fluence of 6.4×10^{11} cm^{-2}. This defect-enhanced charge multiplication (DECM) only appeared when the reverse bias during irradiation ranged from 170 - 1830 V out of a maximum operating bias of 2000 V and the proton flux ranged from 9.8×10^{7} to 3.4×10^{9} cm^{-2}s^{-1}. Values outside of either range led to losses in CCE. It is expected that DECM should be encountered in other devices, especially those with sufficiently high electric fields to cause impact ionization.**

***Index Terms*— Avalanche photodiode (APD), displacement damage, ion beam induced charge (IBIC) technique.**

I. Introduction

AVALANCHE photodiodes (APDs) are high-gain optical sensors which can encounter high levels of radiation in nuclear safeguards, satellites, high-energy physics, and military applications. These devices enable fast and efficient sensing for scintillation detection, light detection and ranging (LIDAR), particle detection, and fiber optic receivers [1-5]. Radiation damage can degrade APD performance and must be accounted for when designing systems and planning missions [6]. Irradiation flux and applied bias are typically insignificant in affecting displacement damage effects in semiconductors, but a growing number of reports have shown that they play an outsized role under certain conditions. This research reports observations by which certain combinations of applied reverse bias and proton irradiation flux in an irradiated APD lead to large increases in its output when tested using the ion beam induced charge (IBIC) technique.

APDs are similar to standard photodiodes, with the advantage of having internal signal multiplication that enhances their signal-to-noise ratio. These devices are structured so that the generated photoelectrons can drift through a region that contains a high electric field, typically above 1×10^{5} V/cm. APDs can operate close to the breakdown voltage without experiencing the destructive effects of avalanche breakdown. Impact ionization occurs in the region with a high electric field and the electrical signal is magnified prior to leaving the diode. The construction of APDs is variable, with some relying on multiple layers of P-type, N-type, and intrinsic silicon, and others consisting of simple PN junctions. The latter is used here.

Cumulative exposure to particle radiation normally raises the noise and leakage currents in semiconductor-based sensors and weakens the signal response to stimuli. The latter is typically quantified after irradiation using the charge collection efficiency (CCE), which may be used to compare the post-irradiation response to a pre-irradiation baseline measurement [7]. Charge collection efficiency is defined in (1) as the ratio of the charge induced in the electrodes over the charge which is liberated by the incident ion.

$$CCE(V) = \frac{Q_{collected}(V)}{Q_{generated}} \tag{1}$$

$Q_{generated}$ is the charge which is found by integrating the electronic stopping power of the ion over its path length. For protons incident on silicon, the generated charge is nearly equal to the incident ion's energy. $Q_{collected}$ is the charge induced in the electrodes following an ion strike. Equation (2) gives the collected charge in integral form and is adapted from an expression from Vittone [8].

$$Q_{collected}(V) = -\int_0^t \int_{\Omega} \left(\boldsymbol{J_n}(\boldsymbol{r}, t') + \boldsymbol{J_p}(\boldsymbol{r}, t') \right) \cdot \frac{\partial \boldsymbol{E}(\boldsymbol{r})}{\partial V}\Big|_V \, d\boldsymbol{r} \, dt' \tag{2}$$

In (2), t is the time required for full charge collection, Ω is the volume, $\boldsymbol{r}$ is the position vector, $\boldsymbol{J}$ gives the current density vector, subscripts n and p denote electrons and holes, respectively, V is the applied bias, and $\boldsymbol{E}$ is the electric field

Manuscript received August 6, 2021; revised November 02, 2021 and December 13, 2021; accepted Dec 17, 2021. This research was performed under appointment to the Nuclear Nonproliferation International Safeguards Fellowship Program sponsored by the Department of Energy, National Nuclear Security Administration's Office of International Nuclear Safeguards (NA-241). This research had been partially supported and conducted by the International Atomic Energy Agency (IAEA), Nuclear Science and Instrumentation Laboratory (NSIL) – Physics Section. (*Corresponding author: R. M. Zedric.*)

R. M. Zedric, C. M. Marianno, and S. S. Chirayath are with the Center for Nuclear Security Science and Policy Initiatives, Department of Nuclear Engineering, Texas A&M University, College Station, TX 77843 USA (e-mail: r.zedric@gmail.com)

Y. Diawara is with the Spallation Neutron Source at Oak Ridge National Laboratory, Oak Ridge, TN 37831 USA

I. Darby is with the School of Physics and Astronomy at the University of Glasgow, Glasgow, G12 8QQ United Kingdom

vector. The partial differential is also known as Gunn's weighting potential and is evaluated at the applied bias V. The equation was modified from its original form to use current densities instead of charge densities and velocity profiles. The charge $Q_{collected}$ has also been expressed as a function of bias.

In an ideal diode at full depletion with no traps and no charge multiplication, CCE is 100%. When impact ionization is present, the current densities will become amplified and will raise the CCE above 100%, which is typical for a pristine APD that is biased within its normal operating range. Once an APD is irradiated, traps and recombination centers will then suppress the CCE. However, it is possible to irradiate an APD and measure CCE values that are above 100% but still below that of pre-irradiation values. In order to present the IBIC results in a more intuitive way, we introduce a ratio of CCE values in (3) called the charge collection ratio (CCR).

$$CCR(V) = \frac{CCE^{irradiated}(V)}{CCE^{unirradiated}(V)} = \frac{Q_{collected}^{irradiated}(V)}{Q_{collected}^{unirradiated}(V)} \quad (3)$$

By expressing IBIC results as a ratio of post- versus pre-irradiation measurements at similar applied biases, the interpretation of data is simplified for biases where the APD gain is higher than 1. CCR values under 100% mean that the effects of irradiation have suppressed the IBIC response through trapping and recombination of charge carriers. CCR values above 100% mean that additional impact ionization occurs within the APD. CCE is presumed equal to the CCR when the gain is negligible, and CCE is used herein to reference work by others.

Abnormal device behavior has been reported in several non-APD devices where the CCE of an irradiated device appears higher than expected, with values sometimes exceeding the pre-irradiation level of 100%. This has been reported in several isolated papers as well as from numerous studies affiliated with the CERN Radiation Hard Semiconductor Devices for Very High Luminosity Colliders (RD50) collaboration. The effects have appeared in several types of materials and devices but only under limited circumstances. Lange et al. have reported a partial recovery of CCE in silicon epitaxial pad diodes after proton irradiation and attributed it to "charge multiplication" within the device [9,10]. Herein, this has been rephrased as defect-enhanced charge multiplication (DECM) to avoid confusion with the normally-occurring levels of band-to-band impact ionization (B2B-II) in unirradiated APDs. Casse et al. have subsequently reported observations of DECM in 2013 after neutron irradiation of silicon microstrip detectors, demonstrating that the effect is not exclusive to ions [11]. Much of the prevailing literature has suggested that DECM was due to defect-induced increases in the electric field near the junction which allowed for impact ionization to occur [12,13]. Vizkelethy has reported in 2017 a much stronger rise in CCE after irradiating a gallium-nitride vertical diode. This device has exhibited an 8-fold increase in CCE following irradiation with silicon ions. Vizkelethy has in turn proposed that the defects themselves were assisting in the process of impact ionization [14]. This process is better known as trap-to-band impact ionization (T2B-II) and it has received a thorough theoretical examination by Robbins in the early 1980's. It is similar in concept to B2B-II except that only one additional carrier is freed instead of two, and the energy threshold is lower than the semiconductor band gap [15-17]. It is not clear what ultimately causes DECM except that it appears related to impact ionization [14].

Observations in this research show that the appearance of DECM in the APD is closely tied to a combination of applied bias and irradiation flux. These parameters are usually considered to be insignificant in the formation of displacement damage and are often omitted from publications on radiation effects [13,18]. However, several past irradiation studies using deep-level transient spectroscopy (DLTS) have shown that bias and flux can independently alter defect production. Hallén has shown that for a constant fluence, simply increasing the proton flux in irradiated silicon from $1x10^7$ to $2x10^{10}$ $cm^{-2}s^{-1}$ will result in fewer vacancy-oxygen (VO), divacancy (V_2), and vacancy-oxygen-hydrogen (VOH) complexes [19]. Other DLTS studies have shown that forward or reverse biases across an irradiated diode will also change the relative concentrations of defects [20-22]. The compounding effects of bias and flux are discussed here in relation to their effects on DECM.

II. Materials and Methods

The target devices used in these experiments were commercially-available APDs produced by Luna Optoelectronics (formerly Advanced Photonix, Inc) with model number 630-70-75-500. Prior studies showed that these APDs performed well in radiation detection as standalone and as scintillator-coupled devices. These were designed with an active area of 2 cm^2 and a peak operating voltage of 2000-V reverse bias. General descriptions of these APDs are found elsewhere [1,23,24]. Spreading resistance measurements were outsourced to give the doping of the APDs. These showed the p-type region had a doping density of $1.05x10^{15}$ cm^{-3}, the n-type region was doped to $7.44x10^{13}$ cm^{-3}, and the junction depth was 17.5-µm below the surface. The bias-dependent response of the APD is shown in Fig. 1, which contrasts manufacturer-provided optical gain values against the measured IBIC response for 1.9-MeV protons [25].

Proton beams were used for both irradiations and subsequent charge collection measurements in this study. Ions were accelerated using 6 MV tandem Van de Graaff and 1 MV Tandetron accelerators and focused into beams approximately 2 µm in diameter using a triplet of quadrupole magnets. These were raster scanned repeatedly across pre-programmed target areas to induce damage or to probe the APD's response. All irradiations were made by raster scanning the beam over 100 µm x 100 µm squares. The scanning speed was optimized so the beam covered an entire square in 1.03 seconds. IBIC measurements used much larger scan sizes to fully encompass one or more damaged regions. Beam energies of 2 and 3 MeV were used for all irradiations and most measurements. 1.9-MeV protons were used for the charge collection measurements shown in Fig. 1 and were not used further. The facility and its capabilities are described elsewhere [26].

Fifty-three irradiations were made on three separate APDs using 2-MeV protons in vacuum. An additional irradiation with

3-MeV protons was made outside of vacuum, where the beam energy was degraded by an aluminum transmission window with a thickness of 3 µm. TRIM calculations showed that the beam energy degraded to approximately 2.93 MeV at the surface of the diode [27]. The 1.5-mm air gap between the foil and the diode helped contribute to beam spreading, but only reduced the beam energy by a few tens of keV.

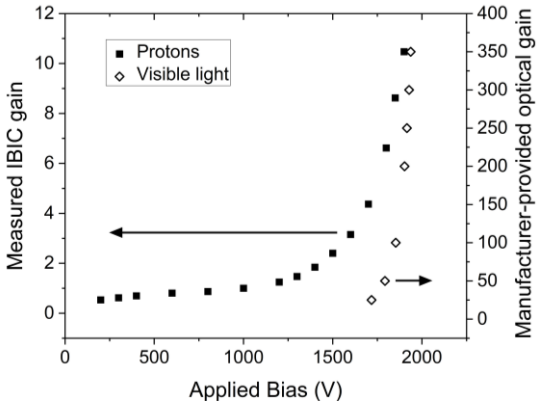

Fig. 1. Bias-dependent APD response to photon and proton stimulation. IBIC charge collection measurements for 1.9-MeV protons are normalized to the 1000 V response. IBIC values are presented as black squares and correspond to the y-axis on the left. Manufacturer-provided optical gain values are shown for biases above 1725 V [25]. These are depicted as open diamonds and correspond to the y-axis on the right. The optical gain curve is steeper than the IBIC response curve because photocurrent can traverse the entire length of the APD's multiplication region, whereas only a portion of the IBIC current passes through the multiplication region.

Ion energies were chosen so that the injected ions would come to rest within the depletion region of the APD. Transport of Ions in Matter (TRIM)-predicted penetration depths in silicon were 48 µm for the 2-MeV beam in vacuum and 90 µm for the 3-MeV beam in air [27]. PADRE modeling predicted that a reverse bias of only 57 V was needed for the width of the depletion region, also known as the space charge region (SCR) to exceed the end of range of a 2-MeV proton beam in vacuum [28]. We calculated that the electric field had almost no effect on the penetration depth of a 2-MeV proton. As each proton moved through the SCR, it experienced an opposing force due to the electric field. Assuming the maximum operating bias of 2000 V was applied, integrating the force over the path length yields approximately 700 eV of work being done on the proton. Stopping and Range of Ions in Matter (SRIM) tables show that 700 eV of kinetic energy will allow a proton to travel approximately 0.013 µm in silicon [27]. It is therefore assumed for this study that the electric field has a negligible effect on the penetration depth of protons.

Early tests were made in sets of 3x3 grids with a spacing of 60-90 µm between regions. Such a tight spacing had been used successfully in PN junction photodiodes by Jakšić et.al [29]. However, the spacing for later experiments was modified when the initial irradiations showed interference with each other. Subsequent irradiations were spaced at least 150-µm apart and were done individually or separated into 3x1 arrays.

The flux, and irradiation biases each spanned orders of magnitude so that their effects could be better understood. The majority of irradiations were made at a fluence of 6.4×10^{11} cm^{-2}, selected to balance beam time allocation with achieving sufficiently measurable damage. Average flux values ranged from 4.6×10^{7} to 1.6×10^{10} cm^{-2}s^{-1}. Irradiations at 6.4×10^{11} cm^{-2} and 1.6×10^{10} cm^{-2}s^{-1} could be completed reliably in under 40 seconds. Longer irradiations beyond 10 minutes sometimes encountered difficulties in maintaining a steady beam current, therefore the average flux value may not be representative of the maximum or minimum fluxes encountered for all tests. Irradiations were performed at 17 different biases from 0 V to 1830 V to test the effects of bias on displacement damage. Bias was held constant during each irradiation with a Canberra 3102D high voltage power supply and a 10 MΩ resistor in series with the APD. Actual voltages across the APD were nearly equal to the biases applied by the power supply. I-V measurements before and after irradiation show such high resistance values from the APD that the 10 MΩ resistor never had more than a few volts across it.

On-line beam monitoring was used to measure flux and fluence. Early experiments were made using low flux values with bias applied so that the total fluence could be measured by counting the pulses in the APD. Simultaneously, a particle-induced x-ray emission (PIXE) detector was calibrated to count the x-rays emitted from protons interacting with silicon [30]. PIXE alone was used to measure irradiation fluence once it was calibrated.

IBIC measurements were used to assess the local effects of damage on the diode. These measurements used 2- and 3-MeV proton beams to make 534 IBIC scans. The majority used 2 MeV protons, while 13 scans used attenuated 3-MeV beams and 4 scans used attenuated 2-MeV beams. As with the irradiations, the IBIC measurements were made by raster scanning a focused beam across the surface of the diode. The beam currents were kept far below a femtoampere and produced between hundreds and thousands of pulses per second. The low beam currents used for IBIC measurements are typically insufficient to cause measurable damage in devices. Beam currents for IBIC scans were measured by directly counting ion strikes in the APD because they were too low for PIXE measurements. Other sources describe the equipment used in these measurements [26]. IBIC responses are presented herein using both CCE and CCR. The former is used where measurement biases were 1000 V or less, and the latter when some or all measurement biases in a set exceeded 1000 V. The two terms are equivalent when impact ionization is negligible in the pre-irradiation baseline measurement.

IBIC scan areas usually extended hundreds of micrometers past the edges of the irradiated regions. Undamaged regions were carefully measured to reduce the uncertainties in calculating CCE and CCR values. IBIC scans were made with various combinations of beam energy, time after irradiation, and reverse bias applied during measurement. The history of applied bias also differed between damaged regions. Measurement biases ranged from 40 to 1900 V and scans were made as quickly as two minutes after an irradiation or up to 4 months later. Scanning times typically lasted minutes or tens of minutes, with longer measurements being used to assess the behavior of damaged regions over time.

The data from IBIC scans were processed to calculate CCE and CCR by averaging the values within energy and spatial regions of interest (ROIs). Representative areas of the damaged regions were taken from the center in order to avoid edge effects [31]. Uncertainties given for CCE and CCR values show a 1σ standard deviation taken from list mode data within the ROIs.

III. Results and Discussion

An irradiation was performed outside the vacuum chamber with a beam of 3-MeV protons. It was followed by multiple IBIC scans with the same beam energy, with the results shown in Fig. 2. The aluminum window attenuated the beam energies to 2.93 MeV and induced some spreading, as is seen in the scans. Limited post-processing analysis was made with these IBIC scans because the beams were diffused and the irradiations were made before accurate fluence and flux measurements were available. The high uniformity of the CCR response in the 500-V scan indicates that full charge collection occurs in the damaged region despite the presence of defects. DECM was clearly visible in the 1200- and 1700-V measurements, with CCR reaching 125% and 149%, respectively. The 1800-V measurement only showed loss in CCR.

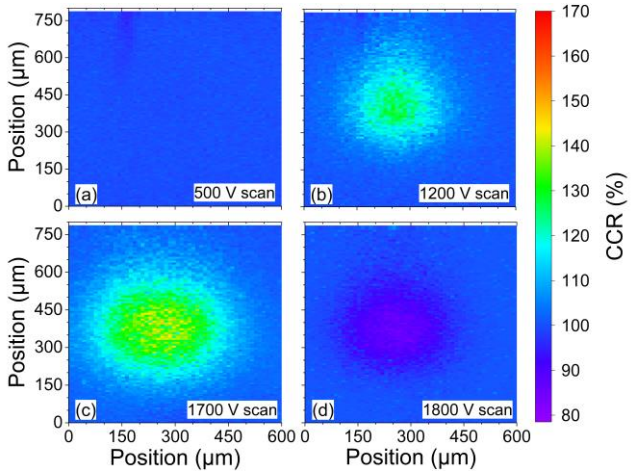

Fig. 2. Observed CCR for four IBIC scans with varying measurement biases. A spot on the APD was irradiated using 3-MeV protons at a reverse bias of 1200 V and was carried out shortly before the measurements. The IBIC scans were measured using 3-MeV protons with reverse biases of 500 (a), 1200 (b), 1700 (c), and 1800 V (d) as shown in the lower right corner of each image. Radiation effects were pronounced in the 1700-V scan but had lesser impacts at other measurement biases.

Following the experiment in air, the APD was moved into the vacuum chamber. A single irradiation was made with 2-MeV protons at 1000 V with fluence and flux values of 6.4×10^{11} cm^{-2} and 3.2×10^{10} cm^{-2}s^{-1}, respectively, and then examined over the next 22 hours. The first IBIC scan recorded after the irradiation is shown in Fig. 3. A horizontal profile from the same scan was taken from the center of the damaged region and is shown in Fig. 4. These figures depict the substantial gain in CCE that is seen when DECM occurs. Figs. 3-6 depict IBIC responses for measurement biases of 1000 V, where impact ionization is minimal and CCE is presumed equal to CCR for this APD.

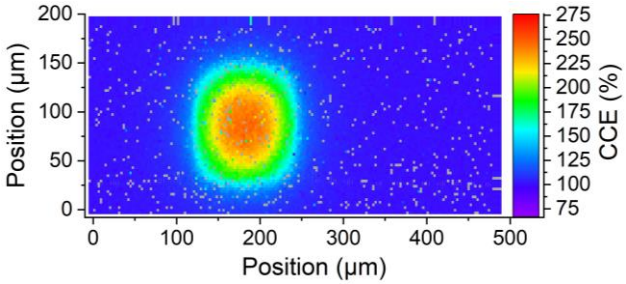

Fig. 3. CCE response from a region irradiated and measured at 1000-V bias. Pixels are gray if an IBIC response was never measured for a particular set of (x,y) coordinates.

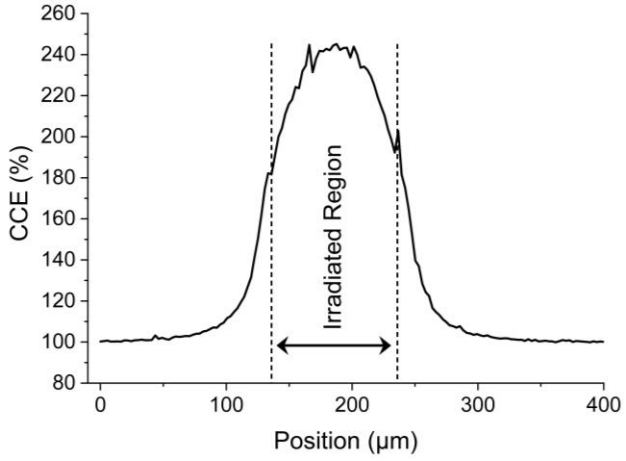

Fig. 4. Horizontal slice of the IBIC data from Fig. 3. The dashed lines show the boundaries of the irradiated region, which was created by raster scanning the 2-µm-diameter beam spot across a 100 µm x 100 µm spot size.

Figs. 3 and 4 each show that DECM began deep inside the irradiated region and stretched far outside of it. Only a small area within the irradiated region had a nearly uniform CCE. It took nearly 100 µm of separation from the central region for the CCE to return to baseline levels. It is not yet understood why DECM extended out so far. TRIM simulations of normally-incident 2-MeV protons in silicon showed that over 99.1% of vacancies formed within a 10-µm radius of the initial ion vector [27]. Electric field bending or defect diffusion likely occurred in order to induce DECM so far beyond the bounds of irradiation. Following the initial scan in Fig. 3, the CCE was tracked continuously for 21 hours while the reverse bias was held at 1000 V. Time-dependent behavior is depicted in Figs. 5 and 6 which illustrates that the presence of DECM is not permanent but can subside with time.

The CCE vs time curve in Fig. 5 shows that the response in the damaged region decreased monotonically over the measurement period. DECM survived the entire measurement period although it dropped substantially during this time. The observed drop contrasted with a steady temporal response of the unirradiated region which was measured several-hundred-µm away. Although it appears that the sharp discontinuity at 900 s suggests an instability in the measurement equipment or experimental conditions, the response of the undamaged region indicates otherwise. Hence, the observed discontinuity is attributable to a physical effect occurring within the diode, such as a sudden restructuring or dissociation of defect clusters near

the ion end of range. Further investigation of the discontinuity and the responsible phenomenon may be of interest. The profiles shown in Fig. 6 reveal additional information about the temporal behavior of the irradiated region. The peaks collapsed in place instead of broadening or narrowing, which suggests that the simple outward diffusion of defects may not be to blame for the loss in DECM. Instead, it is likely due to the interactions between two or more types of defects within the irradiated region. Assuming that DECM is generated due to a single, immobile type of compound defect, the loss of DECM could be attributed to neutralization by a different type of mobile defect. Excess vacancies (V), interstitials (I), and even unbound hydrogen (H) are mobile at room temperature and could contribute to DECM suppression.

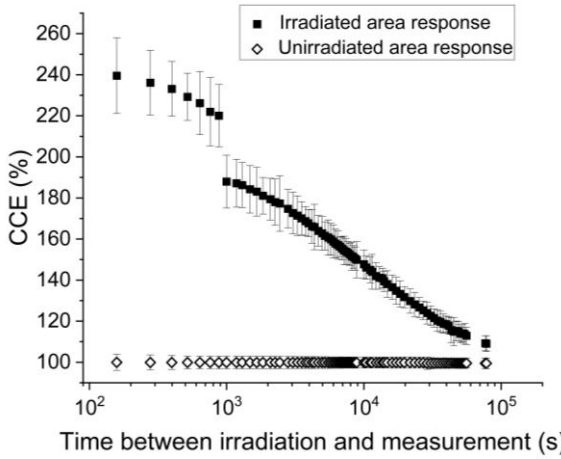

Fig. 5. Time-dependent IBIC responses of an irradiated region exhibiting DECM. This shows the transient behavior of the irradiated and unirradiated regions from Fig. 3 when measured for 21 hours at 1000 V. Black squares show the CCE measured from the center of the damaged region. Open diamonds show the unirradiated response from approximately 200-µm away from the irradiated region. Both responses were measured simultaneously. The apparent discontinuity in the irradiated area response is discussed in the text.

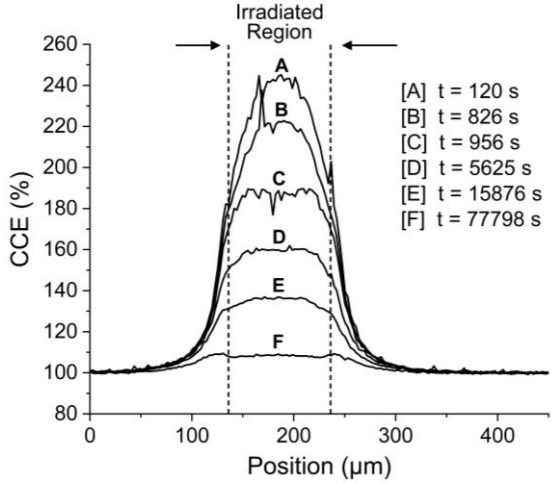

Fig. 6. Progression in DECM degradation with time. The horizontal slice depicted in Fig. 4 is included with five others from different scans to show the spatial and temporal change in CCE. Curves B and C show slices on either side of the discontinuity shown in Fig. 5. The legend shows the elapsed time from the end of the irradiation to the midpoint of the measurement.

Following the end of measurements from Fig. 5, the irradiated region was subjected to different reverse biases to assess in greater detail the effect of measurement bias on the IBIC response. These measurements are shown in Fig. 7. The measurements were conducted after 21 hours to prioritize data collection for Fig. 5.

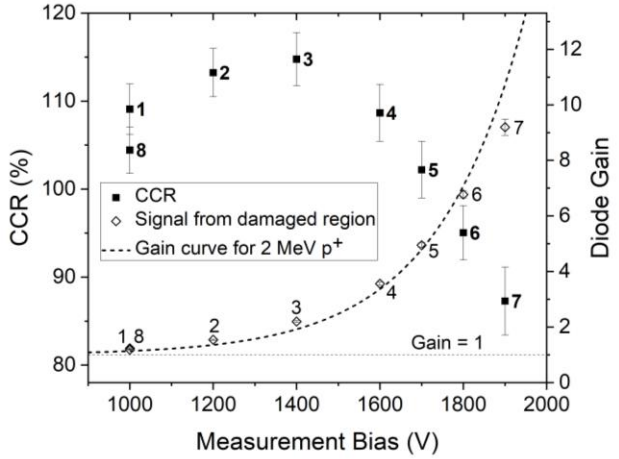

Fig. 7. IBIC response versus bias for the irradiated region in Fig. 3, taken 21 hours after irradiation. The gain (dashed curve) for 2-MeV protons was formed through an exponential fit to IBIC measurements from the surrounding unirradiated region. Open diamonds indicate the gain-normalized signal from IBIC measurements. Black squares represent the CCR. Points are numbered in the order of measurement. CCR and CCE are interchangeable for measurements 1 and 8 because the gain is negligible at 1000 V.

Within Fig. 7, it is seen that increasing the measurement bias led to an increase in CCR up to 1400 V, after which the CCR began to decrease. It dropped below 100% at 1800 V. The presence of DECM at 1000 and 1200 V is notable because impact ionization is typically insignificant in this APD at these biases. The 8th point is a repeat measurement of the 1st and it shows that the CCR at 1000 V dropped by 5% in the hour that it took to perform the entire set of measurements. Figs. 2 and 7 show similar CCR response profiles. In each case, the CCR initially rose with increasing bias, but then subsided below 100% when the bias reached 1800 V. However, the two figures differ in CCR profile shape. Fig. 2 has a higher CCR at 1700 V than at 1200 V, while the opposite is true for Fig. 7.

Numerous additional measurements were made to assess the effects of flux and applied bias during irradiation. These parameters showed a remarkable ability to influence the effects of displacement damage. Fig. 8 shows the clearest results of how both parameters influenced the formation of DECM. It displays the IBIC results from all 53 irradiations made in vacuum with 2-MeV protons. All irradiations at zero bias failed to produce DECM and instead led to damage as is normally encountered in IBIC measurements. Irradiations at sufficiently high fluxes also failed to produce DECM. Irradiations where DECM was observed are shown as black squares. These only occur over a tight range of flux and exclude irradiations made at 50 V or below. The eight irradiations on the right edge of Fig. 8 at 1.6×10^{10} $cm^{-2}s^{-1}$ are compared in Fig. 9 with DECM-producing irradiations to show the effects of flux on displacement damage.

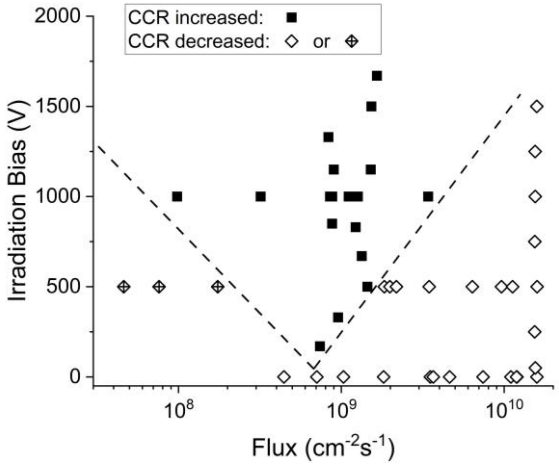

Fig. 8. Effects of applied bias and flux on the appearance of DECM. 53 irradiations with 2-MeV protons in vacuum are represented and are divided into two categories: those with maximum CCR values exceeding 100% and those where CCR never exceeded 100%. Black squares show the former and open diamonds the latter. Measurement biases of either 1000 or 1200 V were used for each data point. The difference in measurement biases is insignificant for this plot because either bias will readily show if DECM is present, as seen in Fig. 7. Flux uncertainties ranged from 1 to 6% except for the three irradiations shown as crossed diamonds at 500-V bias with flux values less than $2x10^8$ $cm^{-2}s^{-1}$. These three irradiations had flux uncertainties up to 33% and their corresponding IBIC results were dissimilar to other observations; see text for details. Dashed lines are presented as a visual guide.

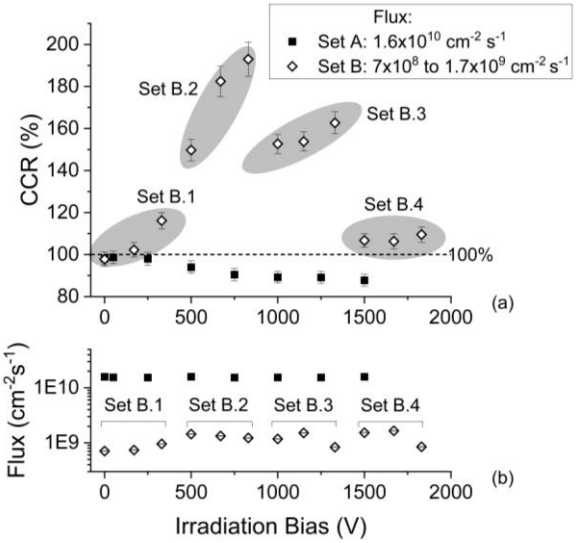

Fig. 9. Effects of irradiation bias and flux on CCR and DECM. The two x-axes give the bias applied during each irradiation. The upper y-axis (a) shows the measured CCR and the lower y-axis (b) shows the flux for each irradiation. Uncertainties in (b) are smaller than the size of the data points. Open diamonds correspond to flux values from $7x10^8$ to $1.7x10^9$ $cm^{-2}s^{-1}$, with subsequent IBIC measurements at 1000 V. Black squares correspond to a flux of $1.6x10^{10}$ $cm^{-2}s^{-1}$, with measurements at 1200 V. Fluence values were $6.4x10^{11}$ cm^{-2}, and fluence and flux uncertainties were between 1 to 2%. DECM is clearly pronounced in the irradiations with lower fluxes and non-zero biases. The small difference in measurement bias has a minor influence on CCR and does not prohibit qualitative comparisons between the two sets.

Both 1000- and 1200-V measurement biases were used for the data within Figs. 8 and 9. The discrepancy in measurement biases was a product of the exploratory nature of this research. Earlier experiments were performed prior to the observation and confirmation of DECM. The 1200-V bias was chosen for early experiments, including for set A in Fig. 9, because the gain at this bias is approximately 1. Later experiments, including set B in Fig. 9, were performed after DECM had been confirmed and studied extensively. This work had been done at 1000 V, so it became a natural choice for further study. Although the data sets were not originally intended to be compared, post-processing analysis demonstrated that irradiation bias and flux acted together to influence the defect behavior. This necessitated that sets A and B be shown together in Fig. 9.

An analysis of the gain and CCR curves in Fig. 7 demonstrates that qualitative comparisons between the 1000- and 1200-V measurements are useful in understanding the behavior of defects. The gain is nearly 1 for each bias, with the value at 1200 V being about 20% higher than the value at 1000 V. Impact ionization therefore played only a minor role in the formation of signals prior to irradiation and the introduction of DECM. Once a region had been irradiated, the gain curve could no longer be relied upon to describe the signal response. However, Fig. 7 again shows a small difference between 1000- and 1200-V measurement biases, with only a 4% difference observed in measured CCR values when DECM was present.

Fig. 9 shows that vastly different behavior occurred between set A with flux values of $1.6x10^{10}$ $cm^{-2}s^{-1}$ and set B with flux values from $7.0x10^8$ to $1.7x10^9$ $cm^{-2}s^{-1}$. The complete absence of DECM in set A is contrasted with the prominent appearance of DECM in set B. Notably, the effects of irradiation at 0 and 50 V were statistically indistinguishable, regardless of flux. The SCR at these biases was smaller and did not overlap with the end of range for a 2-MeV proton. An additional effect is seen in Fig. 9 for set A which shows that the apparent damage is dependent on irradiation bias. The effect is rare but significant [18]. Set A is sampled from a separate experiment and is discussed elsewhere in greater detail [32].

The irradiation bias is thought to influence defect interactions through a combination of charge state manipulation and drift inducement. The defect charge state is controlled by the Fermi or quasi-Fermi levels and it affects defect mobilities and the favorability of defect interactions. V and I defects and unbound H atoms are all mobile in silicon at room temperature. A slight drift can be induced upon charged defects by the electric field. As these defects diffuse, positive defects are nudged towards the anode (surface) and negative defects towards the cathode. It is likely that the electric field promotes the separation or overlap of V, I, and H defects, affecting the density and spatial distribution of stable defects such as V_2, VO, VOH, and vacancy-phosphorus (VP) pairs which are formed [18,20-22,32]. The relative lack of oxygen in the float-zone silicon of the n-type region is also important for promoting defect mobility [33].

Within Fig. 9, sets B.3 and B.4 merit additional attention. The points in sets B.1 and B.2 rise monotonously from 0 to 830 V, after which the CCR falls significantly. However, the CCR does not fall monotonously from 830 V onward, but instead it falls, rises, falls, and rises again. This is an unexpected consequence of the experimental procedure which reveals the presence of yet another phenomenon.

Due to beam time constraints, the experiment for set B was

not performed with single irradiations followed by single measurements. Instead, it consisted of three sequential irradiations, all neighboring each other on the same diode, followed by three sequential measurements of the entire subset. This greatly sped up the experiment and still enabled the comparison of isochronal measurements. However, it relied on the assumption that the CCR for a particular fluence and flux only depended on the irradiation bias, measurement bias, and time after irradiation. This assumption was shown to be wrong because suppression of DECM occurred at higher biases. The history of applied bias between the end of irradiation and the start of measurements became an additional variable that was inadvertently introduced. A review of list-mode IBIC data from Fig. 7 confirmed that post-irradiation bias played a role in DECM degradation. Had time allowed for individual irradiations followed by individual measurements, it is expected that sets B.3 and B.4 would mirror the behavior of B.1 and B.2 and that the entire set would show symmetry.

Except for three observed values seen in Fig. 8, all irradiations at or above 170 V with a sufficiently low flux had exhibited DECM at some point. There appeared to be a bias-dependent flux threshold for producing DECM, with flux needing to be below $1.5\text{x}10^{9}$ $\text{cm}^{-2}\text{s}^{-1}$ when irradiated at 500 V, yet could be as high as $3.4\text{x}10^{9}$ $\text{cm}^{-2}\text{s}^{-1}$ at 1000 V. Further experiments would be needed to clarify this apparent threshold. The largest observed increase in CCE was by a factor of 2.86, for a total of 186% increase in CCE for a region irradiated at 1000 V. In contrast to the high flux, reverse bias cases, damaged regions with DECM showed a strong susceptibility to evolve over time and under the influence of applied bias. An attempt was made to create an empirical equation to describe the CCE with time, but it proved to be unfeasible with the available data. The evolution of defects with time appeared to be responsible for complicating the behavior of CCE after irradiation.

The IBIC response of the APD was studied extensively in this work. However, the optical properties of the APD after irradiation were not measured. Within this particular APD, it is known that photons will deposit their energy and liberate photoelectrons much closer to the surface, allowing photocurrent to travel the entire length of the SCR and the multiplication region inside of it. The photoelectrons will also be able to travel a greater distance before encountering the bulk of defects at 48 μm. For these reasons, we expect a reduced impact from defects and DECM on a measured optical signal. The effects should be independent of photon wavelength for this APD because its construction allows for nearly all optical energy to be deposited outside of the multiplication region.

The mechanism behind DECM is not yet known but evidence suggests that it may be due to T2B-II. Vizkelethy already demonstrated through time-resolved IBIC (TRIBIC) measurements that DECM involves avalanching. In a device with a breakdown voltage above 1700 V, Vizkelethy showed that a modest change in measurement bias from 250 to 350 V could substantially increase the measured TRIBIC signal amplitude from an irradiated region. The measurements also showed that the time duration of the IBIC signal remained the same regardless of bias, suggesting that SCR widening was not a contributing factor to DECM. Since TCAD simulations showed that the carrier drift velocities remained constant, the SCR could not have widened without also increasing the carrier transit times [14]. While SCR widening seems an unlikely culprit, it was not possible to say if DECM was merely caused by an increase in electric field due to the creation of new space charge. Defect concentrations in the APD for a fluence of $6.4\text{x}10^{11}$ cm^{-2} should exceed the N-type doping concentration of $7.44\text{x}10^{13}$ cm^{-3} near the ion end of range, with TRIM simulations predicting defect densities up to 10^{16} cm^{-3}. The presence of space charge could significantly affect the electric field here, promoting additional impact ionization. However, the clear absence of DECM when the irradiation bias is zero or when the ion flux exceeds $1.6\text{x}10^{10}$ $\text{cm}^{-2}\text{s}^{-1}$ makes this seem unlikely. Vizkelethy suggested the most likely cause was that the traps themselves helped to directly facilitate impact ionization by serving as a stepladder for charge to reach the conduction band. This may be the best explanation because of the way DECM manifests in Fig. 7. DECM occurred at biases where impact ionization is not normally produced, suggesting there could be a reduced energy threshold. Hot carriers with insufficient energy for B2B-II would have been capable of causing T2B-II if the right defect was present.

The downward curve in CCR in Fig. 7 from 1400 to 1900 V is attributed to the significant role that B2B-II normally plays within this bias range. The gain for an undamaged APD increases from 2 to 11 over this bias range, where high electric fields and high carrier velocities lead to B2B-II. However, the distribution of traps and charged defects within the damaged region of an irradiated APD causes a significant reduction in the local carrier lifetime and carrier mobility. This reduces the net carrier velocity in the vicinity of the defects. This is expected to suppress B2B-II and the gain curve enough to fully account for the downward CCR trend from 1400 to 1900 V. Although DECM can raise the CCR, it appears insufficient to compensate for the loss in B2B-II. If T2B-II occurs, its contributions at higher biases could be limited by the density and availability of defects with the right charge states. Additionally, T2B-II produces one additional charge carrier while B2B-II produces both an electron and a hole. Further work is needed to clarify why DECM is produced. Drift-diffusion modeling of the APD's response is an important next step.

IV. Conclusions

Radiation effects studies on a commercial APD demonstrated vulnerabilities which may appear in these devices when used in nuclear safeguards, satellites, and military applications. Post-irradiation measurements showed that applying reverse bias during irradiation led to large increases in CCE up to 186% above baseline levels. DECM appeared following irradiations with both 2- and 2.93-MeV protons. It manifested over a subset of applied reverse biases from 170 to 1830 V and average irradiation fluxes ranging from $9.8\text{x}10^{7}$ to $3.4\text{x}10^{9}$ $\text{cm}^{-2}\text{s}^{-1}$. The flux range which led to DECM was wider when tested at 1000 V and narrower when tested at 500 V. Additionally, the magnitude of the increase in the IBIC response was greatest when irradiation and measurement biases

were near 1000 and 1400 V, respectively.

DECM proved to be a transient effect which could endure for hours. The longest continuous measurement of 22 hours showed that DECM lasted nearly a day when the APD was continuously held at 1000 V. This means that DECM can disrupt or compromise performance in APDs for short term missions after being irradiated. The time-dependent CCE response of an irradiated device is desirable to know for situations such as this. However, the complexity of this process appeared too great to describe using a simple empirical relation. Further studies are needed to untangle the complicated behavior of DECM with time.

ACKNOWLEDGMENT

All accelerator experiments were carried out thanks to the hard work and long hours by the staff and scientists, especially Milko Jakšić, within the Division of Experimental Physics at the Ruđer Bošković Institute. The authors would also like to thank Dr. Lin Shao at Texas A&M University, Natko Skukan in NSIL at the IAEA, and Ed Bielejec and Gyorgy Vizkelethy at the Ion Beam Laboratory at Sandia National Laboratories who generously contributed invaluable insights and guidance.

REFERENCES

[1] M. Moszyński, M. Kapusta, M. Balcerzyk, M. Szawlowski, D. Wolski, I. Węgrzecka, M. Węgrzecki, “Comparative study of avalanche photodiodes with different structures in scintillation detection,” *IEEE Trans. Nucl. Sci.*, vol. 48, no. 4, pp. 1205-1210, Aug. 2001.

[2] T. F. Refaat, G. E. Halama, R. J. DeYoung, “Characterization of Advanced Avalanche Photodiodes for Water Vapor Lidar Receivers,” NASA Langley Res. Ctr., Hampton, VA, USA, NASA/TP-2000-210096, Jul. 1, 2000.

[3] D. K. Barton, R. Falcone, D. Kleppner, F. K. Lamb, M. K. Lau, H. L. Lynch, *et al.*, “Report of the American Physical Society Study Group on Boost-Phase Intercept Systems for National Missile Defense: Scientific and Technical Issues,” Rev. Mod. Phys, vol. 76, no. 3, pp. S1-S424, Oct. 2004.

[4] T. Szumlak, “Silicon detectors for the LHC Phase-II upgrade and beyond RD50 Status report,” *Nucl. Instrum. Methods Phys. Res. A.*, vol. 958, p. 162187, Apr. 2020.

[5] J. C. Campbell, “Recent Advances in Avalanche Photodiodes,” J. Lightw. Technol., vol. 34, no. 2, pp. 278-285, Jan. 2016.

[6] E. Garutti, Yu. Musienko, “Radiation damage of SiPMs," *Nucl. Instrum. Methods Phys. Res. A.*, vol. 926, pp. 69-84, May 2019.

[7] M. B. H. Breese, "A theory of ion beam induced charge collection," J. Appl. Phys., vol. 74, no. 6, pp. 3789-3799, Sept. 1993.

[8] E. Vittone, “Theory of ion beam induced charge measurement in semiconductor devices based on the Gunn’s theorem,” *Nucl. Instrum. Methods Phys. Res. B.*, vol. 219-220, pp. 1043-1050, Jun. 2004.

[9] J. Lange, J. Becker, E. Fretwurst, R. Klanner, G. Lindström, “Properties of a radiation-induced charge multiplication region in epitaxial silicon diodes,” *Nucl. Instrum. Methods Phys. Res. A.*, vol. 622, no. 1, pp. 49-58, Oct. 2010.

[10] J. Lange, J. Becker, D. Eckstein, E. Fretwurst, R. Klanner, G. Lindström, “Charge collection studies of proton-irradiated n- and p-type epitaxial silicon detectors,” *Nucl. Instrum. Methods Phys. Res. A.*, vol. 624, no. 2, pp. 405-409, Dec. 2010.

[11] G. Casse, D. Forshaw, T. Huse, I. Tsurin, M. Wormald, M. Lozano, G. Pellegrini, "Charge multiplication in irradiated segmented silicon detectors with special strip processing," *Nucl. Instrum. Methods Phys. Res. A.*, vol. 699, pp. 9-13, Jan. 2013.

[12] S. Kuehn, “RD50 Collaboration overview: Development of new radiation hard detectors,” *Nucl. Instrum. Methods Phys. Res. A.*, vol. 824, pp. 422-425, Jul. 2016.

[13] J. R. Srour, J. W. Palko, “Displacement Damage Effects in Irradiated Semiconductor Devices,” *IEEE Trans. Nucl. Sci.*, vol. 60, no. 3, pp. 1740-1766, Jun. 2013.

[14] G. Vizkelethy, M. P. King, O. Aktas, I. C. Kizilyalli, R. J. Kaplar, “Nuclear microprobe investigation of the effects of ionization and displacement damage in vertical, high voltage GaN diodes,” *Nucl. Instrum. Methods Phys. Res. B.*, vol. 404, pp. 264-268, Aug. 2017.

[15] D. J. Robbins, “Aspects of the Theory of Impact Ionization in Semiconductors (III),” Physica Status Solidi B, vol. 98, no. 1, pp. 11-36, Mar. 1980.

[16] D. J. Robbins, P. T. Landsberg, “Impact ionisation and Auger recombination involving traps in semiconductors,” J. Phys. C: Solid State Phys., vol. 13, no. 12, pp. 2425-2439, Apr. 1980.

[17] D. J. Robbins, “Multiphonon broadening of impact ionisation and Auger recombination involving traps in semiconductors,” J. Phys. C: Solid State Phys., vol. 16, no. 19, pp. 3825-3840, Jul. 1983.

[18] M. S. Robbins, L. Gomez Rojas, “An Assessment of the Bias Dependence of Displacement Damage Effects and Annealing in Silicon Charge Coupled Devices,” *IEEE Trans. Nucl. Sci.,* vol. 60, no. 6, pp. 4332-4340, Dec. 2013.

[19] A. Hallén, D. Fenyö, B. U. R. Sundqvist, R. E. Johnson, B. G. Svensson, "The influence of ion flux on defect production in MeV proton irradiated silicon," J. Appl. Phys., vol. 70, no. 6, pp. 3025-3030, Sept. 1991.

[20] C. Liu, X. Li, H. Geng, E. Rui, J. Yang, L. Xiao, “DLTS Studies of bias dependence of defects in silicon NPN bipolar junction transistor irradiated by heavy ions,” *Nucl. Instrum. Methods Phys. Res. A.*, vol. 688, pp. 7-10, Oct. 2012.

[21] Y. N. Erokhin, J. Ravi, G. A. Rozgonyi, “In situ electric field perturbations of deep trap accumulation in silicon during proton ion implantation,” Appl. Phys. Lett., vol. 66, no. 13, pp. 1656-1658, Mar. 1995.

[22] R. A. Brown, J. Ravi, Y. Erokhin, G. A. Rozgonyi, C. W. White, “Charge state defect engineering of silicon during ion implantation,” MRS Proc., vol. 439, pp. 131-136, 1996.

[23] M. Moszyński, M. Szawlowski, M. Kapusta, M. Balcerzyk, “Large area avalanche photodiodes in scintillation and X-rays detection,” *Nucl. Instrum. Methods Phys. Res. A.,* vol. 485, no. 3, pp. 504-521, Jun. 2002.

[24] L. M. P. Fernandes, F. D. Amaro, A. Antognini, J. M. R. Cardoso, C. A. N. Conde, O. Huot, et al, “Characterization of large area avalanche photodiodes in X-ray and VUV-light detection,” J. Instrum., vol. 2, no. 8, Aug. 2007, Art. No. P08005.

[25] Luna Optoelectronics, “Non-cooled large area DUV silicon avalanche photodiode,” SD 630-70-75-500 datasheet, 2018.

[26] M. Jakšić, I. Bogdanović Radović, M. Bogovac, V. Desnica, S. Fazinić, M. Karlušić, *et al.*, "New capabilities of the Zagreb ion microbeam system," *Nucl. Instrum. Methods Phys. Res. B.*, vol. 260, no. 1, pp. 114-118, Jul. 2007.

[27] J. F. Ziegler, M. D. Ziegler, J. P Biersack, “SRIM - The stopping and range of ions in matter (2010),” *Nucl. Instrum. Methods Phys. Res. B.,* vol. 268, pp. 1818-1823, Jun. 2010.

[28] M. R. Pinto, K. Smith, M. A. Alam, S. Clark, X. Wang, G. Klimeck, D. Vasileska, “PADRE,” NanoHUB, Aug. 2014. [Online] Available: https://nanohub.org/resources/padre Accessed on: Jan 15, 2021.

[29] M. Jakšić, Z. Medunić, N. Skukan, M. Bogovac, D. Wegrzynek, "Fabrication of a Si Photodiode for Position Sensitive Radiation Detection," *IEEE Trans. Nucl. Sci.*, vol. 54, no. 1, pp. 280-283, Feb. 2007.

[30] P. Pelicon, J. Simčič, M. Jakšić, Z. Medunić, F. Naab, F. D. McDaniel, “Spherical chamber – effective solution for multipurpose nuclear microprobe,” *Nucl. Instrum. Methods Phys. Res. B.*, vol. 231, no. 1, pp. 53-59, Apr. 2005.

[31] B. L. Doyle, G. Vízkelethy, D. S. Walsh, "Ion beam induced charge collection (IBICC) studies of cadmium zinc telluride (CZT) radiation detectors," *Nucl. Instrum. Methods Phys. Res. B.*, vol. 161-163, pp. 457-461, Mar. 2000.

[32] R. M. Zedric, S. S. Chirayath, C. M. Marianno, Y. Diawara, N. Skukan, “Bias-dependent displacement damage effects in a silicon avalanche photodiode,” *Nucl. Instrum. Methods Phys. Res. B.*, vol. 507, pp. 42-45, Nov. 2021.

[33] A. Bates, M. Moll, “A comparison between irradiated magnetic Czochralski and float zone silicon detectors using the transient current technique,” *Nucl. Instrum. Methods Phys. Res. A.*, vol. 555, no. 1-2, pp. 113-124, Dec. 2005.